LBNL-2001613

Complementary Subsurface Characterization Methods to Develop a Geologic Model for the EGS Collab Experiment, Sanford Underground Research Facility

W. Roggenthen[1], T. Kneafsey[2], J. Burghardt[3], T. Doe[4], C. Hopp[2], T. Johnson[3], C. Ulrich[2], P. Schwering[5], N. Uzunlar[1], and the EGS Collab Team

Abstract

The EGS (Enhanced Geothermal Systems) Collab project was performed within the Sanford Underground Research Facility (SURF) with a goal of understanding processes and evaluation of models related to hydraulic stimulation of rock at depth. The present work deals with the development of Testbed 2 where experiments were conducted at a depth of 1.25 km and were located within a well-characterized testbed in a metamorphic, amphibolite host rock. A total of eleven boreholes varying in length between 10.6 m and 81.2 m were continuously cored to develop the testbed. In addition to the continuous coring of the amphibolite host rock, geophysical instrumentation supporting electrical resistivity tomography (ERT), microearthquake (MEQ) detection, and optical fiber providing distributed temperature sensing (DTS) and distributed acoustic sensing (DAS) were installed in the monitoring boreholes, all of which produced a comprehensive complementary suite of characterization and monitoring technologies. Pre-stimulation characterization of the groundwater conditions identified only two hydraulically significant fractures, neither of which transects the central portion of the testbed. Flow and pressure monitoring indicated low pre-existing pore pressure conditions likely affected by the mine openings. The ERT proved to be especially useful in identifying where the injected water was being transmitted whereas the MEQ data gave indications of what was happening physically in the rock because of the introduction of the injected water. This testbed was developed in a host rock with a uniform lithology, but which had undergone previous deformation producing fractures which could be made more hydraulically transmissive. One of these northwest trending fractures was able to transfer injection water away from the initial hydraulic fracture system to a more remote location where microearthquake measurements identified the development of a major injection plane. The drift from which the boreholes were drilled experienced minor inflow due to injection water which is interpreted to have been transported through east-west pre-existing natural fractures. Although as much as 25% of the injected water was recovered by nearby boreholes in the testbed as planned, the major inflow into the drift was provided through a fracture defined by MEQ activity.

Keywords: geothermal, microearthquakes, electrical resistivity tomography, fractures

[1]South Dakota School of Mines & Technology, Rapid City, South Dakota, USA ,[2]Lawrence Berkeley National Laboratory, Berkeley, California, USA, [3]Pacific Northwest National Laboratory, Richland, Washington, USA, [4]Doe Geo, Redmond, Washington, USA, [5]Sandia National Laboratories, Albuquerque, New Mexico, USA

1.0 Introduction

The EGS (Enhanced Geothermal Systems) Collab Project established two testbeds within the Sanford Underground Research Facility (SURF) to support experiments focused on the predictions related to hydraulic fracturing for geothermal research. SURF is a subsurface facility located in the central U.S., and, although large-scale physics experiments are an important part of its mission, the facility hosts numerous experiments and projects requiring an underground environment ranging from physics laboratories to geoscience and engineering projects (Heise, 2015). The EGS Collab project testbeds were used for studies related to hydraulic fracturing supporting investigations for geothermal research whose goals, results, and overall geologic environment were described by Kneafsey and others (2020; 2021; 2022; 2023). EGS Collab Testbed 1 was developed at a depth of 1.5 km on the 4850 Level of SURF, and EGS Collab Testbed 2 was constructed at a depth of 1.25 km on the 4100 Level of the facility. The results from the work in Testbed 1 were summarized previously (Fu and others, 2021; Kneafsey and others, 2020), but the present discussion is limited to the development of a geologic model of EGS Collab Testbed 2 on the 4100 Level of SURF. The

specific goals of the work at Testbed 2 focused on stimulation of natural fractures using hydraulic injection and injection strategies that investigated the effects of varying injection rates. It was found that significant shear stimulation was not evident and that the resulting hydraulic fractures required hydraulic propping to be maintained (Kneafsey and others, 2024). Interpretation of these results is assisted by an understanding of the geologic environment, including natural fractures of the testbed, and describing this environment is the major purpose of the present discussion.

The part of the project discussed here focuses on the geologic environment in which the testbed was developed, i.e., prior to conduct of the fracturing experiments. The array of geophysical and geological complimentary techniques installed by the project provided an excellent database to perform characterization and to develop such a geologic model. Development of Testbed 2 began with drilling a 50 m deep vertical hole (TV4100) in which a hydraulic fracturing experiment was conducted as part of the early characterization of the stresses in the testbed. Based upon this experiment, it was possible to determine the direction of the minimum compressive stress in the testbed and to infer the preferred induced fracture directions (Burghardt and others, 2022; Ulrich and others, 2022). The determination of the in situ stress guided the borehole design such that they were generally normal to the minimum stress direction. Therefore, a selected volume of rock in the subsurface was examined using eleven drill holes (Fig. 1a) with lengths varying between 10.6 m (TH4100) and 81.2 m (E2-TS). The 96 mm diameter holes (HQ size) were cored continuously, and the core had a nominal diameter of 63.5 mm with recovery approaching 100 percent, e.g., E2-TC had a 99.6 percent core recovery. Many of the holes were outfitted with a range of geophysical instrumentation including hydrophones, accelerometers, electrode arrays for electrical resistivity tomography (ERT), and fiber for distributed temperature sensing (DTS) and distributed acoustic sensing (DAS). The holes also were subjected to a wide range of downhole wireline measurements that allowed direct comparison of the petrophysical properties of the rock with the core recovered from the drilling. The instrumentation was described in more detail by Kneafsey and others (2022).

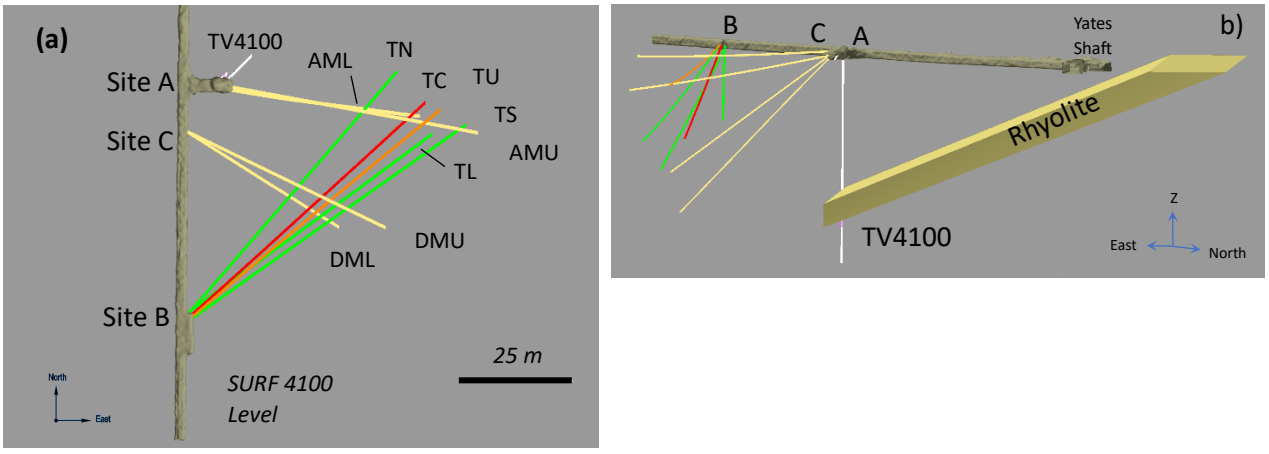

Figure 1. a) Plan view of the borehole layout in EGS Testbed 2 on the 4100 Level (1.25 km depth) showing the four monitoring holes, AMU, AML (Site A), DMU, and DML [Site B), and TN, TU, TC, TL, and TS (Site B). The Site B holes were used primarily for injection of water and for production of the injected fluid. Holes TV4100 (vertical) and TH400 (horizontal) were drilled to establish how the overall testbed should be developed. b) Oblique view showing the relation between the boreholes and a rhyolite body that was encountered during the drilling of TV4100. The updip extension of this rhyolite is exposed in the 4100 Drift. Drift is a term used for a horizontal excavation that is much longer than it is wide and that does not have an opening to the surface on either end.

The 4100 Level Testbed 2 holes have plunges varying from vertical to 1.5° with an average of 18°, excluding the one vertical hole and one short horizontal hole drilled at Site A (Fig. 1). The two longer holes at Site A (AML; AMU) and the two holes at Site C (DML; DMU) were used for geophysical monitoring (two at Site A and two at Site C), and five production/injection boreholes were used as part of the fracturing experiments (Site B). The vertical (TV4100) and horizontal (TH4100) boreholes provided information on the rock mass geology and mechanical rock properties and were used in designing the later nine boreholes in the experimental area. An alcove was excavated at Site B to provide room for a total of five boreholes as well as the equipment for the injection of water at high pressures to perform the fracturing and thermal monitoring experiments. The monitoring and characterization systems produced an extensive, complimentary data set that employed a variety of geophysical methods. This allowed production of an integrated picture of the physical characteristics at the 10-m scale. Much of the data presented here was sourced from the Geothermal Data Repository *(https://gdr.openei.org/egs_collab)* and integration of these data allowed a geologic model to be constructed for the testbed.

2.0 Host Rocks

The host rock is a Precambrian age amphibolite known as the Yates Member of the Poorman Formation that is generally massive as exposed in the drift, although it shows weak layering toward the stratigraphic top of the unit and contains small folds near Site B. A pre-development photo montage of the drift comprising the total extent of the experiment area showed no evidence of water entering the drift and demonstrated that natural fractures were not conducting water prior to the injection of water during the experiment.

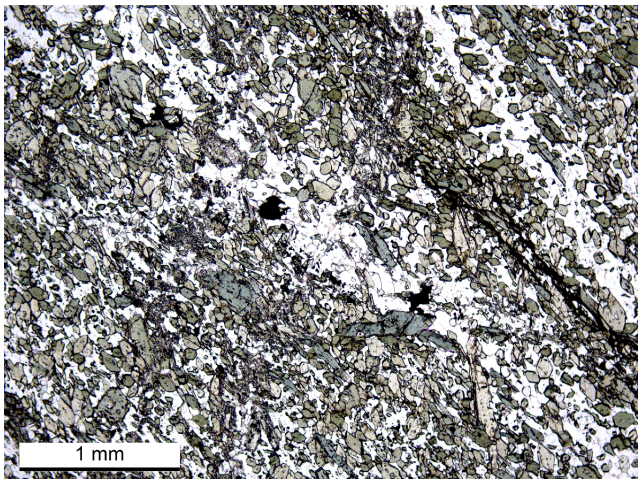

Figure 2. Photomicrograph of amphibolite in plane polarized light acquired from TV4100 at a depth of 19.2 m from the hole collar at Site A. The amphiboles and chlorite are fine-grained and are well aligned which imparts a distinct planar fabric to the rock.

The petrologic texture of the host rock is shown in Figure 2 which is a photomicrograph of a thin section in plane polarized light from a depth of 19.2 m in TV4100. The amphiboles and chlorite in the thin section are well aligned, and the section also shows a small veinlet in the middle of the photo. Semi-quantitative X-ray diffraction analysis (XRD) of amphibolite from 50.3 m in TV4100 is listed in Table 1. The mineralogy of the testbed amphibolite is consistent with the metamorphism of a pre-existing basalt as interpreted by Cady and others (1991). The typical composition of the Yates Unit as described by Cady and others is similar to the values in Table 1 with the exception that the Testbed 2 amphibolite has higher amounts of chlorite. The effect of the greater amounts of chlorite is seen in the occasional development of minor shearing in the core. The unit also contains six thin (5-10 cm thick) sulfide-rich layers within the ~150 m length of the 4100 Level drift encompassing the EGS project area. The bulk of the cores consist of massive amphibolite showing little obvious layering with frequent healed fractures filled with a mixture of calcite

and quartz. Zones with closely spaced fractures occur that sometimes have isolated pore spaces of <1-2 mm in width that are interpreted to be of Tertiary age and are associated with rhyolite intrusions in the area. At least one core shows brecciation, and alteration zones 1 m wide or less occur infrequently, and some zones were hydrothermally altered to the point of creating clays derived from the original amphibolite composition. Two Tertiary-age rhyolites were intersected in the vertical borehole (TV4100, Site A). The first was a 0.6 m layer at 31.9 m and the second was encountered at a depth of 33.6 m and had a thickness of 7.6 m as measured in the vertical borehole. It is likely that these two intersections are from the same intrusion and are connected nearby. Presumably, the same rhyolite body also is exposed in the drift (a term used to describe a horizontal excavation with limited width and no opening to the surface) on the 4100 Level near the Yates Shaft Station, and it is probably the updip continuation of the rhyolite encountered in TV4100 as shown in Figure 1b. The overall orientation of the rhyolite is anomalous in that the dip is shallower than most of the other rhyolites in the SURF underground which typically have dips between 60^{o} and vertical (Noble, 1948). The low-plunging boreholes used in the monitoring and injection/production experiments were designed to remain above the rhyolite and were successful in avoiding the intrusive body.

The rhyolite in Testbed 2 exposed near the Yates Shaft in the 4100 Level drift consists primarily of potassium feldspar, quartz, albite, and finer grained ground mass with phenocrysts of quartz and feldspar. This rock at the Yates Shaft location experienced only minor alteration, and the semi-quantitative XRD analysis is listed in Table 1. The rhyolite encountered in TV4100, however, is extensively altered, and feldspars were consumed producing kaolinite along with precipitation of calcite and preservation of the resulting porosity demonstrating that this portion of the body underwent intensive interaction with fluids. Table 1 lists an XRD analysis of the altered rhyolite encountered in TV4100 from a depth of 38.6 m below the 4100 Level drift floor.

Table 1. Semi-quantitative XRD analysis of rhyolites and amphibolite in EGS Testbed 2. Rhyolite samples are located with respect the 4100 Level Drift at Site A and the updip exposure of the rhyolite body near the Yates Shaft.

Rhyolite *(wt %)*	***K-Feldspar***	***Quartz***	***Na-Feldspar***	***Clay***	***Calcite***	***Pyrite***	***Muscovite***
Rhyolite exposed near Yates Shaft (unaltered)	47.6%	29.4%	20.1%		1.2%	1.0%	0.6%
Rhyolite – 38.6 m depth TV4100 (altered)	35.2%	28.9%	18.8%	15.5%	1.6%		

Amphibolite	***Amphibole***	***Chlorite***	***Feldspar***	***Quartz***
Amphibolite - 50.3 m depth TV4100	59%	25%	15%	0.5%

3.0 Lidar Imagery

A lidar scan of the area of Testbed 2 imaged the effects of fracturing upon the shape of the drift and analysis of the fractures and is a commonly used technique (Kumar and others, 2023; Singh and others, 2023). However, the fracture directions are biased by the orientation of the drift and favored the east-west fracture systems (Fig. 3a). Injection of water in the boreholes drilled from Site B caused water leakage into the drift in several areas although they tended to be diffuse, and it was difficult to determine their exact

locations except for the area labelled as “main flow” in Figure 3a which had the greatest flow rate. The locations of the fractures providing the inflow became more obvious after injection ceased and the site of the weeps dried because they were marked by white precipitates (Fig. 3b). Although many fractures can be identified in the scanning and inflows were produced during injection, evidence of water inflow into the drift prior to injection of water during the experiments was not observed.

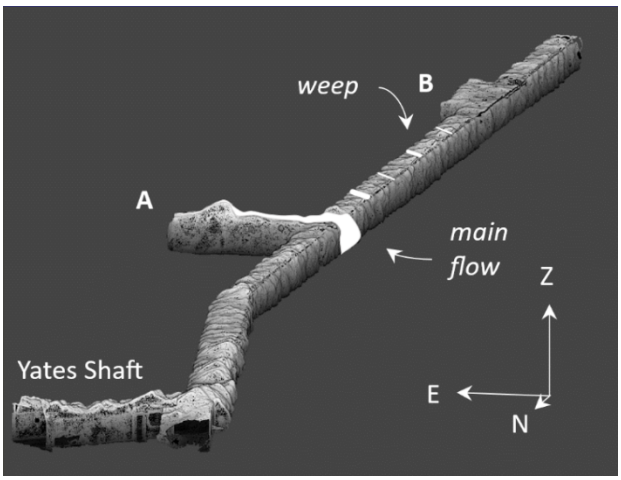

Figure 3a. Lidar image of the 4100 Drift in the vicinity of Testbed 2 and the locations of drilling sites A and B. Weeps are locations where water leaked into the drift due to the injection of water as part of the experiment activities. The location of the weep photographed in Figure 3b is shown, as well as the position with the greatest flow.

Figure 3b. Weeps in drift are marked by precipitate from dissolved solids in the water entering the drift (arrow points to intersection of a precipitate zone with the drift). The intersection of this fracture on the drift wall (Fig. 3a) can be followed across the ceiling although it does not have a clear expression on the right hand wall in the photograph.

4.0 Pre-Stimulation Hydrogeology of the Experiment 2 Testbed

Natural fractures play important roles in EGS development. They may be conductive prior to stimulation or, they may be opened during the stimulation process. The presence of naturally conductive fractures prior to stimulation was assessed through the following activities:

- Flow and shut-in tests on TV-4100
- Integration of observations including core and geophysical logging to identify key fractures in the testbed.
- Monitoring water inflow and outflow from boreholes during drilling Testbed 2
- Single packer pulse tests to determine the permeability of the testbed rocks.

Groundwater flow in the regions of the SURF facility where the EGS Collab experiments were carried out is typified by widely spaced conductive fracture zones with minor seepage at excavation walls and local fracture networks that are isolated or poorly connected to groundwater sources or mine workings. Stetler’s (2016) compilation of data from the DUSEL characterization work of the late 2000’s describes a flow system with few connected fractures with variable pore pressures ranging from 15% to 60% of the hydrostatic gradient from the surface. Testbed 2 on the 4100-foot level is in a dry section of the mine, the nearest seeps being ~70 m south of the testbed near the contact with the overlying upper Poorman Fm. Mapping of the drift identified an open fracture near Site A that was non-flowing and hydraulically isolated.

Only three naturally conductive fractures were identified during the pre-stimulation characterization program, two of which were naturally flowing. OTV logs and drilling records determine the depths of the flow and the orientations of the fractures, and none of these fractures appeared to traverse the central portion of the testbed.

Flowing water appeared in TV-4100, the vertical exploration borehole drilled at Site A. This borehole produced <0.1 liter/min water flow from a fracture in the rhyolite dike. Pressure buildup tests recovered to approximately 100 psi (0.7 MPa or ~6% of hydrostatic). A second flowing fracture appeared near the end of the last test-bed borehole drilled, E2-DMU. This fracture was encountered at a measured length of 49.7-49.9 m (163.0-163.3 feet) with a fracture pole orientation of 336°, 10°. The flow rate from this fracture was ~500 ml/day (0.3 ml/min). Televiewer logs show the flowing porosity is not a single open fracture but small openings (vugs?) in brecciated rock adjacent to a prominent quartz vein. A third likely conductive fracture zone with vuggy porosity in a brecciated zone was encountered in E2-AML between 56.9 m and 57.4 m with measured pole orientations of 158°,25° and 168°, 30°. This fracture zone did not produce water and is likely disconnected from water sources. The locations of these zones are shown in Figure 9b.

Water flows were carefully monitored from each hole every workday during the drilling program to record the depths and magnitudes of water flows and to identify possible connections between boreholes. Except for E2-DMU, all the water flows were into the rock rather than production from the rock with rates between 21 to 177 ml/day during drilling and 0 to 114 ml/day after drilling. Evaporation was ruled out as a cause of water loss, and water losses suggest the testbed rock has been largely depressurized to underground excavations.

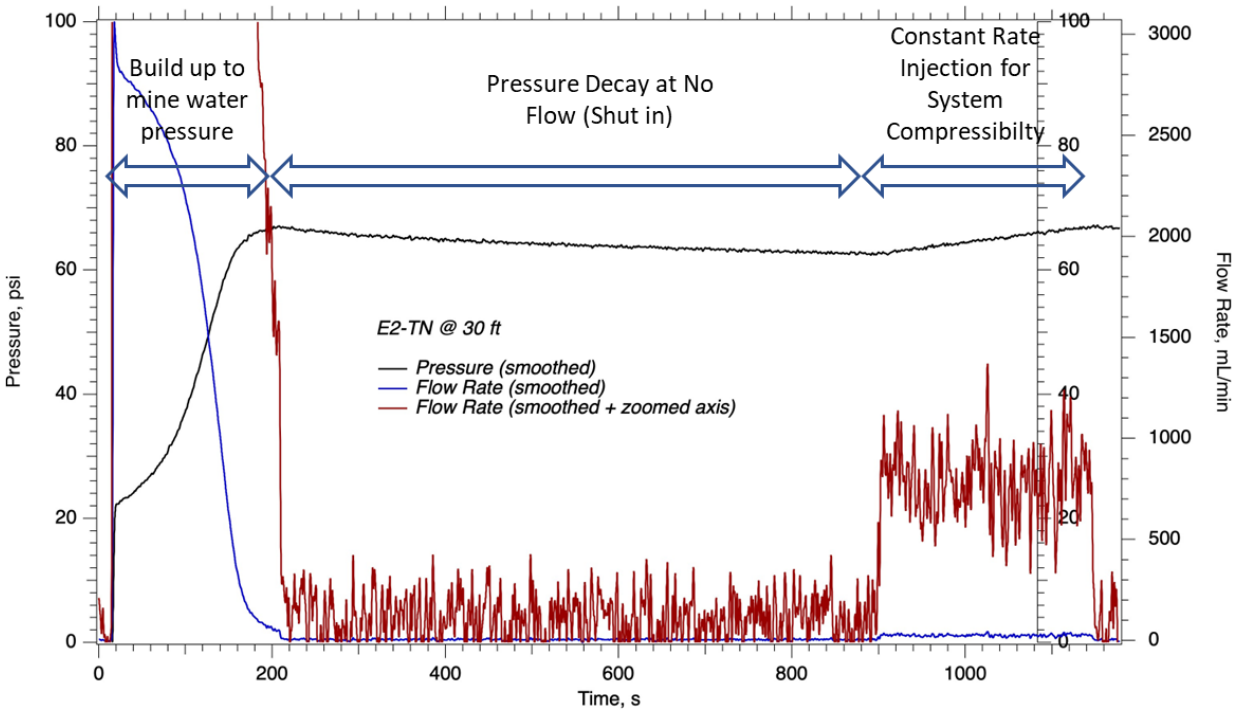

Figure 4. Pressure pulse test. The test started by setting the packer and building up the test zone to mine water pressure (~0.5 MPa, 70 psi). Then the zone was "shut in" and the pressure decayed as water flowed into the rock. After 30 minutes of pressure decay, the injection resumed at 25 ml/min. The pressure buildup indicated the compressibility of the test zone. From the compressibility and pressure decay the water loss volume and the rate of flow were calculated. Assuming approximate steady flow, the transmissivity could be determined from the flow rate and the pressure change (converted to hydraulic head).

Single-packer tests were run over the open lengths of all boreholes along with three additional tests at various depths in E2-TC, the planned stimulation hole. An example of the methodology used is shown in Figure 4. The inferred permeability values for the tests run over the open hole lengths ranged from 2.9 E-18 to 7.1E-19 m^2 with the exception E2-DMU, which had a permeability of 1.5E-16 m^2 owing to the presence of its flowing natural fracture.

Overall, the results of the hydraulic characterization program indicated that the 4100 level testbed is largely free of naturally conductive fractures, and stimulation activities required creating new hydraulic fractures or stimulating non-conductive natural fractures.

5.0 Wireline Logging

5.1 Electrical Resistivity and Sonic Logging

Ulrich and others (2022) described the petrophysical logs that were run in each of the boreholes of Testbed 2. The downhole suite included resistivity, gamma, fluid temperature and conductivity, full-wave sonic, and optical and acoustic televiewer logs. These logs, in addition to the continuous coring of all the holes, allowed the testbed to be characterized in terms of composition, structure, and electrical and acoustic properties. Electrical resistivities greater than 10,000 ohm-m were common due to the minimal porosities, although thin zones of lower resistivity occur in all the holes. The electrical resistivity logs along with optical televiewer logs were used to identify zones for hydraulic fracturing experiments performed by the project.

Determinations of the P and S-wave velocities from the full wave sonic log allowed calculation of the dynamic elastic modulus (E). An example of the relationships between petrophysical logs and core from borehole E2-TC is shown in Figure 5 and Figure 6. The resistivity is plotted as a solid line and the corresponding elastic moduli is a dashed line. An example of the fabric of the bulk of the core material is shown in a section beginning at a distance from the hole collar of 23.5 m in hole E2-TC, and it is massive with few healed fractures (core diameter is 63.5 mm). In contrast, the core section beginning at 41.5 m (b) corresponds to a resistivity low and has smaller values of elastic moduli and closely spaced fractures, although it does not show obvious pore space. In the case of the section beginning at 58 m (zone d), the fracturing is accompanied by a color change and hydrothermal alteration which can proceed all the way to production of illite. The pattern, therefore, is one in which higher fracture frequency led to lower resistivities due higher water content and lower values for E resulting from the physical fracturing. When fracture densities based upon core examination are plotted against the resistivity, the zones of greater fracturing usually correspond to zones of lower resistivity, although the low resistivity can be caused by changes in mineralogy, such as by higher sulfide content. The arrow at 12 m in the figure shows an example where the lower resistivity in hole TC does not correspond to a low in the elastic modulus, and it is attributed to the presence of a sulfide-rich layer.

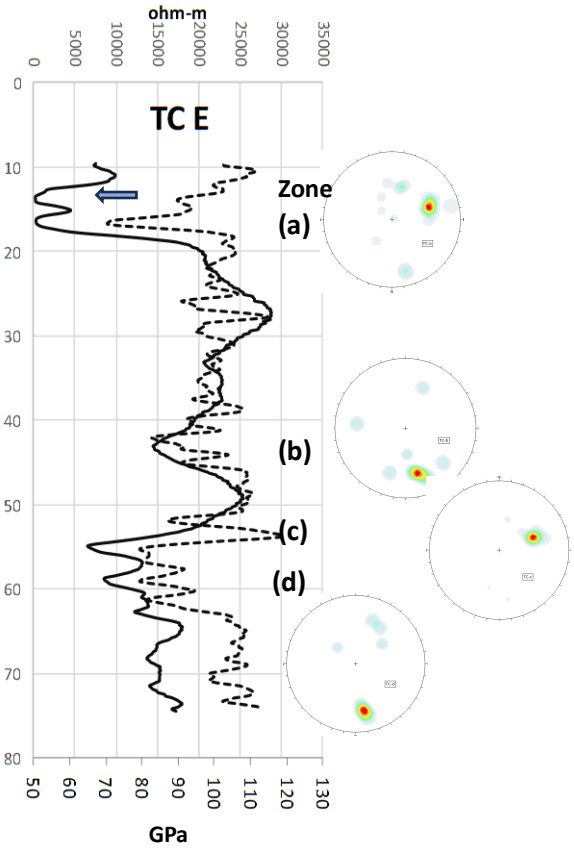

Figure 5. Downhole petrophysical logs from E2-TC. Solid line is electrical resistivity (ohm-m), and the dashed line is the elastic moduli. The arrow points to zone (a) as an example of the relationship between lower resistivity zones and the fracture direction specific to that interval.

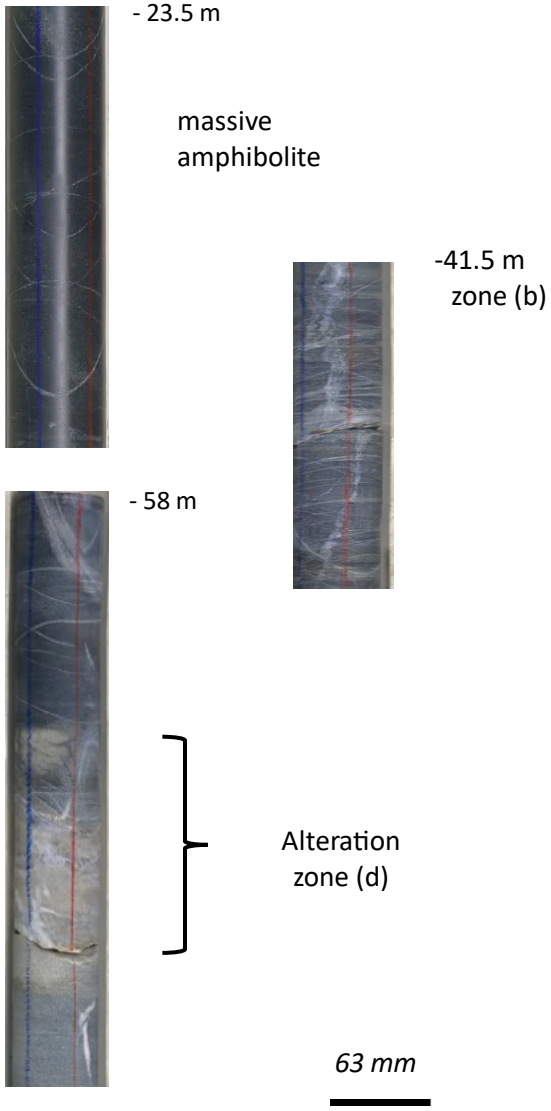

Figure 6. Rock core specific to the downhole logs shown in Figure 5. The top core is from a non-fractured part of the hole. The core from 41.5 m depth shows a portion of a fracture labelled as "b", and the bottom core (58 m) shows the effect arising from an altered section at 58 m depth.

The elastic moduli (E) were used to correlate fracturing capable of transmitting fluids between the boreholes of Site B. Although resistivities could be correlated between the holes, the elastic moduli were useful in that they provided sharper and better defined anomalies for the correlations in identifying. Figure 7 shows the relationship between elastic moduli values and electrical resistivities for hole E2-TU and, in this case, they are nearly identical. In many instances, however, zones of lower resistivity appear to consist of two or more intervals of lower elastic moduli thus providing additional definition.

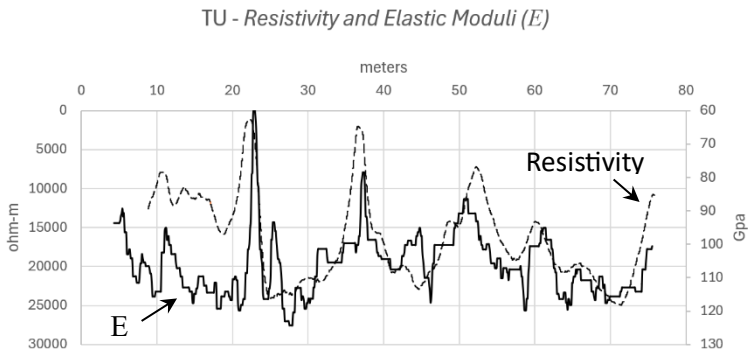

Figure 7. Comparison of elastic moduli with electrical resistivity for hole E2-TU showing that the lower resistivities correspond to lower values of the moduli. The moduli differentiated the inferred fractures better and were used for correlation of fractures between holes.

5.2 Optical Televiewer (OTV)

Downhole optical televiewer (OTV) logging was performed on the boreholes, and the directions of the fractures were determined from the oriented images (Ulrich and others, 2022). Although orientations of fractures throughout the length of the boreholes were determined in their study, only fracture zones previously identified by electrical and OTV logging were used for the present investigation. This resulted in recognizing three distinct orientations from these zones based on their poles in equal area stereographic projections (Fig. 8), and each fracture zone in the core was often characterized by only one dominant fracture set. For the purposes of this discussion, the three orientations are referenced as Fracture Sets 1, 2, and 3. Set 1 fracture poles are restricted to the northeast quadrant, Set 2 occur in the southern hemisphere of the diagrams, and Set 3 plots in the west-northwest portion of the figure, all of which are orthogonal.

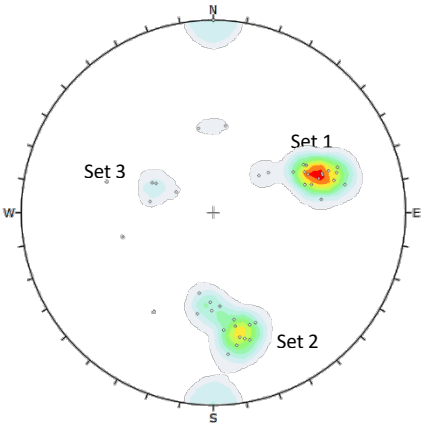

Figure 8. Stereographic plot of orientations from only the fractures identified using petrophysical and OTV logging.

Although many fracture directions occur in the boreholes, restricting the plots to the zones of low resistivity/high fracture density results in these well-defined maxima whose average directions can be associated with the individual fracture zones. Figure 5 shows an example of the relation between the lower resistivity zones and the fracture directions for those intervals. The upper part of Zone (a) in the figure is interpreted to be a mineralogical effect, but the remaining anomalies are ascribed to increases in fracturing although mineralogical effects cannot be ruled out in all instances. Even though the resistivities in the fractures are lower, they are still usually greater than ~4000 ohm-m, which could be due to the existence of only small amounts of porosity or to being thin in relation to the investigated volume provided by the 32-inch electrode spacing of the logging instrument chosen for the plots. This spacing was selected

to minimize potential influences of well bore damage and to promote the detection of steeply dipping fractures that may not have intersected the borehole as suggested by Goldberg and Burgdorff (2005) in their investigation of fracturing in the Palisades Sill.

Using the information from the OTV, which yielded fracture orientations and the identification of relevant fractures from the logging, two maps were prepared. One shows orientations for Fracture Set 1 (Fig. 9a) and the other for Fracture Set 2 (Fig. 9b) located at the intersections of the fractures in the boreholes based upon resistivity anomalies. Set 1 forms a well-defined trend to the northwest, and three lineation directions are shown in Figure 9a.

The trend of the western fracture zone is 330° and it is vertical, but its direction is poorly constrained because the boreholes are spatially close together at this point, and it is shown as a dashed line. The middle zone has an orientation of 344.5° 85.5° NE (dip direction 74.5°), and the eastern zone is oriented at 153.4° 84.8° SW (dip direction 243.4°). These directions are consistent with general structural trends in the underground, such as many of the rhyolite intrusives, as noted by Noble (1948), as well as a nearby major shear zone. Set 2 has several trends (Fig. 9b) but, in general, the trends appear to be capable of supplying water to the weeps observed in the drift.

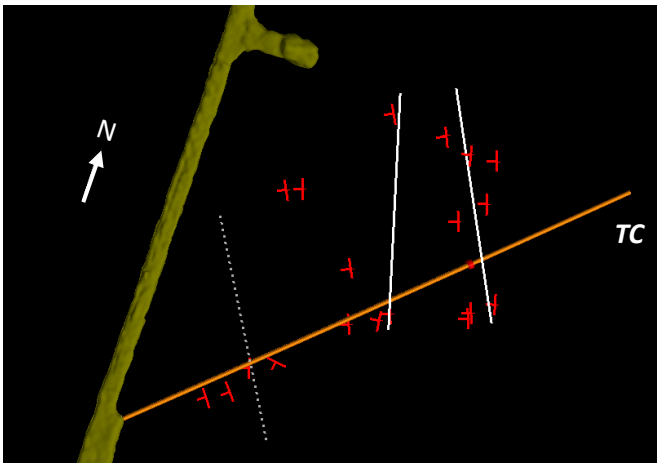

Figure 9a. Fracture Set 1 showing the northwest trend of the fracture system identified in Figure 5. The best development is seen in the easternmost fracture whereas the western trend (dashed line) is more poorly constrained.

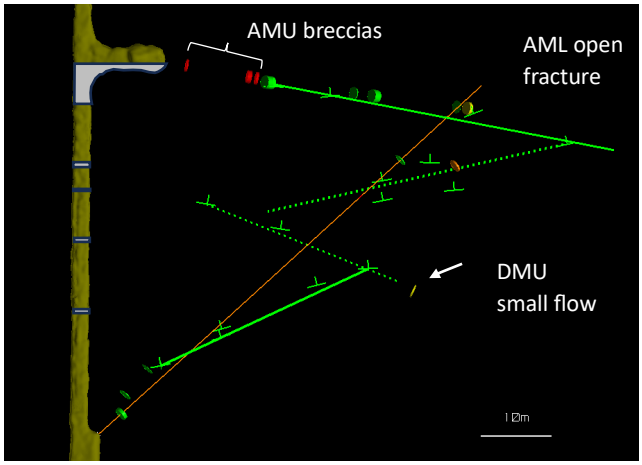

Figure 9b. Fracture Set 2 is represented moderately well in the downhole petrophysical data, and a series of east-west fractures are shown in the figure. These types of fractures may deliver the water entering the drift (weeps shown in gray) during the injection experiments. Intervals of interest in the core includes alteration (green, breccias (red), open fracture in AML, a clay interval in TL, and a small fracture that flowed in DMU. These occurrences lie outside of the test volume as defined by the monitoring boreholes.

6.0 Electrical Resistivity Tomography (ERT) Results

ERT data were used in the investigations for both EGS Collab Testbed 1 on the 4850 Level (Johnson and others, 2021) and Testbed 2 on the 4100 Level (Johnson and others, 2022) with excellent results. Kneafsey and others (2023) summarized the acquisition of the ERT data in Testbed 2 that yielded time-stepped three dimensional images of the electrical structure within the testbed while water was being injected. Electrode

arrays were installed permanently in the four monitoring boreholes in the 4100 Level experiment area as well as holes E2-TN, TU, and TL for portions of the experiments. Electrical resistivity data were collected throughout the injection operations, but a time of particular interest occurred during an early phase of injection in May 2022, when fresh water was injected at a rate of 5 l/min (Schwering and others, 2023). Figure 10 shows the envelope of the change in electrical resistivity between May 05 and May 19, 2022, resulting from injecting water into the testbed, and $Log_{10}(E_{May19}/E_{May05})$ for values greater than 0.15 are plotted in the diagram.

The May ERT data shows several features that were produced by the injection into borehole TC at a measured depth of 50.4 – 51.1 m. Water was injected in TC and moved to (1) which probably represented an accumulation of water adjacent to the injection point. Water then appeared to be transported through a northwest trending fracture to (2) which is near the plane defined by the MEQs (Fig. 11a, b). The prominent elongate region at (3) grew during the injection, but projection of the elevated conductivity of the elongated anomaly at (3) westward into the 4100 Level Drift showed evidence of only small amounts of white precipitate on the drift wall at that location. Therefore, the anomaly at (3) did not appear to be a major contributor to flow. Region (2) appears to be a feeder for this volume, and the northern end of the feeder at (2) is close to an area of brecciation described in core from hole AMU. The anomaly at (2) imaged in the May data has a circular cross-section rather than a planar morphology suggesting that it represents a flow channel developed because of water injection along areas of higher permeability within the planar fracture system. Hyman (2020) noted that the development of such fingers is typical of flow within host rocks with low permeability. This effect may have been favored by the low injection rates used in this experiment which did not exceed 5 l/min (Schwering and others, 2023) as this would have less of a tendency to enlarge the injected system into the fracture planes. Alternatively, the apparent shape may have been influenced by the configuration of the monitoring holes so the possibility of creation of geometric artifacts cannot be eliminated.

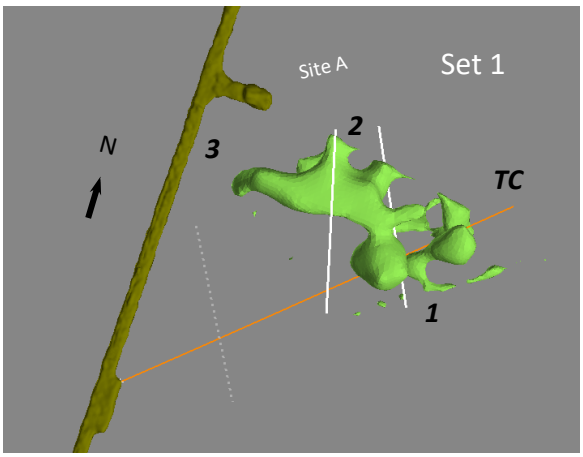

Figure 10. ERT images from May 2022. Water injected into borehole TC moved into a northwest trending fracture at (1) and was transported to (2) which is coincident with a plane defined by MEQ activity (Fig. 10 a, b). Small feeders appear to supply a larger anomaly at (3) that grew during the injection of the water. The anomaly at (3) probably was not a major part of the system, however, because only minor evidence of water was seen in the drift even though (3) was near to the drift wall.

7.0 Microearthquakes (MEQ)

Determinations of MEQ locations were conducted in the EGS Testbed during May 2022, using the four monitoring boreholes: AML, AMU (Site A) and DML, DMU (Site C) and were reported by Hopp (2023) and Kneafsey and others (2023). The early time MEQ location data in the latter part of May 2022 were most useful and were collected when the injection rate increased to 5 l/m. The MEQ locations grouped well,

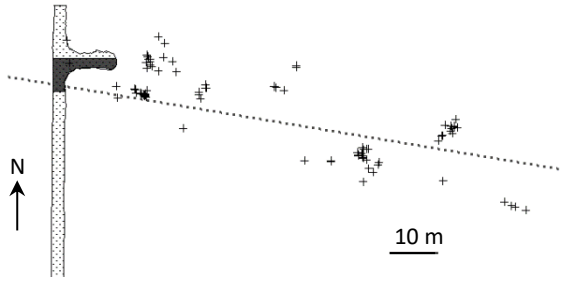

Figure 11a MEQs occurring during late May 2022. Plan view in reference to the 4100 Level Drift and Site A. The dark area in the figure is the location of the point of major inflow into

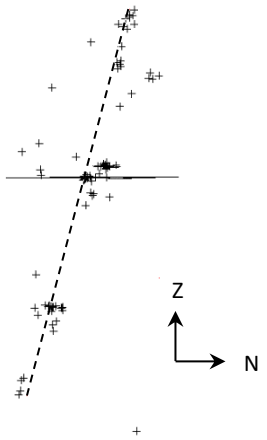

Figure 11b. Side view of the MEQ locations in Figure 11a. The best fit plane strikes 99.6° and has a dip of 74.6° SW.

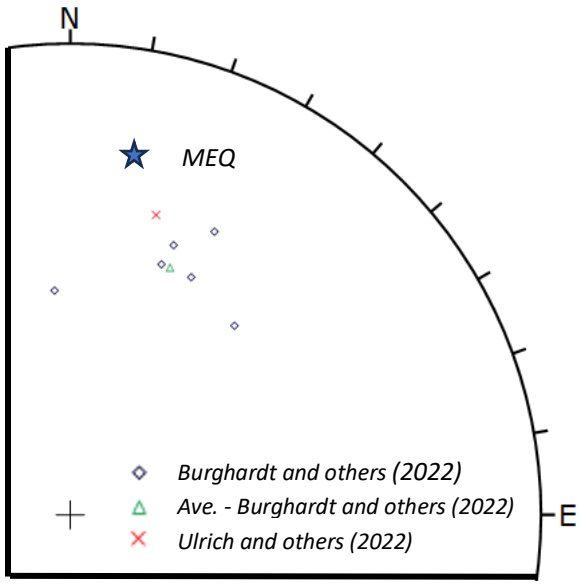

Figure 11c. Northeast quadrant of an equal area stereogram showing directions of minimum compressive stresses determined from measurements in borehole TV4100 at Site A (Burghardt and others, 2022; Ulrich and others, 2022) along with the direction of the best fit plane derived from the May 2022, MEQ data.

and the day-to-day locations were consistent. Toward the end of May as injection continued, the MEQ locations became more chaotic and affected larger volumes of the testbed. The side view of the best fit plane for the early time data is shown in Figure 11b along with the plane orientation, and the plan view is shown in Figure 11a. The MEQs are distributed in a plane with a strike of 99.6° (dip direction 189.6°) and a dip of 74.6° SW in an elongated ellipse with a major axis of approximately 95 m and a minor axis of 24 m. The axis of the ellipse had a plunge of 65.9°. The plane defined by the MEQs intersects the drift where the maximum water into the drift was observed. The pole from the average MEQ plane is plotted in Figure

11c along with the poles for the hydraulic fracturing experiment in TV4100 conducted during the first phase of the experiments in Testbed 2. The pole from the average MEQs plots near the orientations determined from the TV4100 data indicating a close relationship with the minimum compressive stress direction.

8.0 Discussion

The range of techniques used to characterize the testbed on the 4100 Level of SURF, including field and core examination, downhole logging geophysics, downhole geophones and accelerometers, and electrical resistivity tomography provided an opportunity to understand the geologic environment found in a small volume of crystalline rock at the tens of meters scale. Examination of cores, downhole electrical resistivities, and sonic velocities led to the conclusion that fractures affecting the flow of injected water could be identified consistently within the testbed, although some lower resistivity values encountered in the unfractured host rocks were due to the presence of electrically conducting sulfides.

The plane defined by the MEQs was important in capturing water and delivering it to the drift as well as moving it onwards into the formation. The plane dips towards the west, and its orientation is consistent with the measured direction of the current minimum compressive stress from the EGS Collab work in TV4100 (Fig. 11c). The location of the plane defined by the MEQs is remote from where the injection occurred in the boreholes. Although the injection water may have travelled through the northwest-trending natural fractures and encountered an existing favorably oriented natural fracture, it is more likely that the plane defined by the MEQs represents a newly created fracture resulting from the injection of water in the testbed boreholes.

Although speculative, the development of the MEQs in this location remote from the site of injection may be related to the geometry and history of the excavation of the 4100 Drift in that area, portions of which have been open for >70 years (Mitchell, 2010). The plot in Figure 12 was derived from wireline measurements of the fluid temperature in hole AML drilled from Site A which is 10 m east of the main 4100 drift, and hole DML drilled from Site C. The data are plotted in relation to distance from the east side of the 4100 Drift for purposes of comparison. AML and DML have bearings within 25^{o} of each other and their plunges are 39^{o} and 35^{o}, respectively. The times between drilling and logging are similar as well in that AML was logged one month after drilling and DML was logged after 1.5 months. The curves show the effect of cooling due to the presence of the drift, and they begin to converge upon the inferred temperature of the undisturbed rock mass. However, the end of the excavation at Site A is further to the east than Site C which causes AML to be cooler than DML at distances <40 m from the drift wall, and projection of the inferred NW flow path (Fig. 9a) intersects the MEQ plane at ~28 m from the edge of the drift. White and others (2018) and Fu and others (2018) produced simulations of the induced fracture geometries in EGS Collab Testbed 1 on the 4850 Level (1.5 km depth) that resulted from cooling in the drift due to ventilation since the excavation of the 4850 Drift. Their simulations indicated that the thermal/mechanical environment associated with the drift would cause fractures to be drawn into the drift, that effects should be more pronounced closer to the drift, and that fractures would deviate from the ideal penny-shape and become elongated. Although speculative, the effects calculated in the simulations are consistent with many of the features exhibited by the flow into the drift at Testbed 2 and the locations determined for the MEQs. The elongate MEQ plane comes within less than 3 m of the southeast corner of the easterly extension at Site A, and the major inflow into the drift occurs directly at the southeast corner of that feature suggesting that the cooling effect may have initiated and promoted the induced fracture plane.

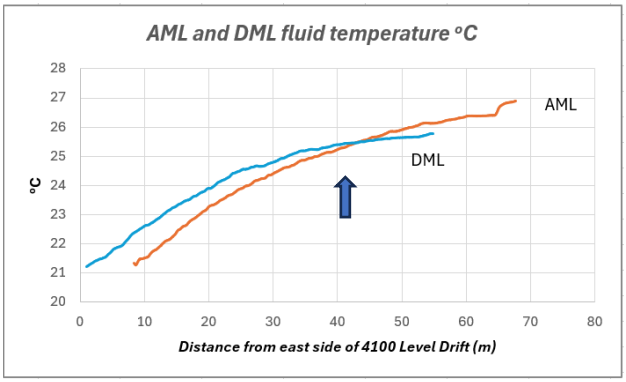

Figure 12. Comparison of fluid temperatures based on wireline logging for boreholes AML (Site A) and DML (Site C) in relation to the east side of the 4100 Drift. At distances <40 m AML found a lower temperature than DML, presumably due to the presence of the excavation extending toward the east which affected the local temperature environment even though AML appears ultimately to find higher temperatures further out in the rock mass. The arrow shows the approximate distance between the drift wall and the inferred location of the NW -trending flow feature in Figure 9a.

Three dominant natural fracture directions were identified in the OTV data. One system trends to the northwest and the other is generally east-west, but evidence of the third fracture system occurs primarily in areas in the northeastern portion of the experimental volume so not as much spatial data is available to analyze this system. Correlation of the NW trending system was accomplished using a combination of resistivity and elastic moduli lows in conjunction with core examination. As a result of the correlation of these anomalies it was found that the northwest trending fracture system is expressed in the three major fractures as shown in Figure 13. They consist of an eastern fracture (153.4° 84.7° SW dip direction 243.4°), a middle trend (344.5° 85.5° NE dip direction 74.5°) , and a western fracture trend (330° 89.7° NE dip direction 60°). The northeast trending fractures are consistent with the observations of Noble (1948) who noted that most of the rhyolite dikes in the area strike a few degrees west of north and typically dip toward the east. This is also the orientation for a major shear zone found further to the west in the underground, which has a dip of 60° to the east. This shear zone produced large amounts of water during mining and demonstrated that it was capable of high hydraulic transmissivities even at depths of more than 2 km (Bowden, 1993). The east-west trending fracture system is not as well developed, but based upon observed water leaking into the nearby drift, smaller amounts of water were introduced into the east-west fracture system that delivers water to the drift south of the major inflow near Site A. Although major conductive features such as these fracture sets occur elsewhere in the SURF underground, the hydraulic testing performed in Testbed 2 demonstrated that permeabilities were small and that the testbed volume was generally free of naturally conductive fractures prior to the injection experiments.

The path of the injected water shown in Figure 13 can be followed from the point where it was injected to where it produced major induced fracturing in the testbed based on the MEQ detections. Injection of water must have produced induced fractures in the immediate vicinity of the injection site, although only 20-25% of the injected water was recovered in the adjacent production boreholes (Burghardt and others, 2022). The major northwest-southeast fracture found through OTV analysis is also seen in the ERT data, and this important fracture carried much of the injected water, although other fractures may have been active outside of the imaged volume. The results from the combined techniques show that the flow of water from the injection went from the injection point through several paths of which at least two involved hydraulically fractured rock.

The impact of the pre-existing fracture system on the flow of injected water in EGS Testbed 2 is important when considering other possible geothermal reservoirs. Older crystalline rock terrains with long and complicated geologic histories may be the site of future geothermal projects and the natural fractures can affect the flow of the injected fluids. Even though the geologic model in this project is well constrained, uncertainties remain. Future geothermal projects may not be able to support the breadth of techniques

used here, and some of the techniques may offer less information as the size of the investigated volume increases.

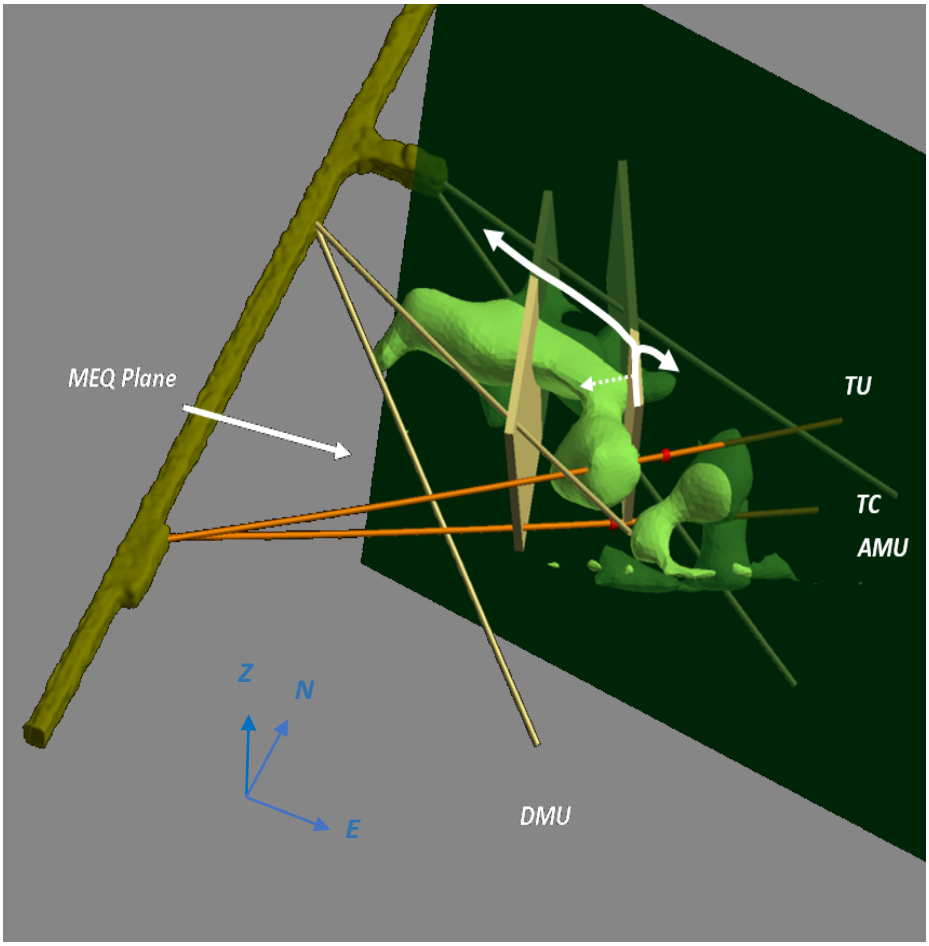

Figure 13. Flow of injected water in Testbed 2 from where it was injected into borehole TC. The main portion of the flow traveled to the northwest through the pre-existing natural fracture until it was delivered to the plane identified by MEQ activity. The fracture identified from the downhole wireline logging and core examination coincide with the linear ERT anomaly showing the location of the water flow. Smaller flows were fed into an east-west pre-existing fracture system that allowed water to be delivered to the locations of smaller inflows into the 4100 Level drift.

9.0 ACKNOWLEDGMENTS

This material was based upon work supported by the U.S. Department of Energy, Office of Energy Efficiency and Renewable Energy (EERE), Office of Technology Development, Geothermal Technologies Office, under Award Number DE-AC02-05CH11231 with LBNL and other awards to other national laboratories. The United States Government retains, and the publisher, by accepting the article for publication, acknowledges that the United States Government retains a non-exclusive, paid-up, irrevocable, world-wide license to publish or reproduce the published form of this manuscript, or allow others to do so, for United States Government purposes. Sandia National Laboratories is a multimission laboratory managed and operated by National Technology & Engineering

Solutions of Sandia, LLC, a wholly owned subsidiary of Honeywell International Inc., for the U.S. Department of Energy's National Nuclear Security Administration under contract DE-NA0003525. This paper describes objective technical results and analysis. Any subjective views or opinions that might be expressed in the paper do not necessarily represent the views of the U.S. Department of Energy or the United States Government. The field work was conducted in the Sanford Underground Research Facility (SURF), which is a federally-sponsored research facility, under Award Number DE-SC0020216. Use of Maptek Vulcan™ in analysis and preparation of the data is appreciated and acknowledged.

10.0 References Cited:

Bowden, Jay A., 1993, The North Homestake Project: Chapter 36 - Mining Application in *Rapid Excavation and Tunneling Conference Proceedings - 1993*, 16 p.

Burghardt J., Knox, H.A., Doe, T., Blankenship, D., Schwering, P.C., Ingraham, M., Kneafsey, T.J., Dobson, P.F., Urich, C., Guglielmi, Y., and Roggenthen, W., 2022, EGS stimulation design with uncertainty quantification at the EGS Collab Site, ARMA 22-2224, *56th Rock Mechanics/Geomechanics Symposium Santa Fe, New Mexico, USA.*

Caddey, S. W., Bachman, R. L., Campbell, T. J., Reid, R. R., and Otto, R. P., 1991, The Homestake Gold Mine, An Early Proterozoic Iron-Formation-Hosted Gold Deposit, Lawrence County, South Dakota . U. S. Geological Survey Bulletin 1857-J, *Geology and Resources of Gold in the United States*, 67 p.

Fu, P., M. White, J. Morris, T. Kneafsey, and EGS Collab Team, 2018, Predicting Hydraulic Fracture Trajectory Under the Influence of a Mine Drift in EGS Collab Experiment I, in *PROCEEDINGS, 43rd Workshop on Geothermal Reservoir Engineering*, edited, Stanford University, Stanford, California.

Fu, P., Schoenball, M., Ajo-Franklin, J. B., Chai, C., Maceira, M., Morris, J. P., et al., 2021, Close observation of hydraulic fracturing at EGS Collab Experiment 1: Fracture trajectory, microseismic interpretations, and the role of natural fractures. *Journal of Geophysical Research: Solid Earth, 126, e2020JB020840. https://doi.org/10.1029/2020JB020840*

Goldberg, D. and Burgdorff, K., 2005, Natural fracturing and petrophysical properties of the Palisades dolerite sill, in *Petrophysical Properties of Crystalline Rocks,* Harvey, P.K., Brewer, T.S., Pezard, P.A., and Petrov, V.A. (eds.), *Geological Society, London, Special Publications, 240*, 25-36.

Heise, J., 2015, The Sanford Underground Research Facility at Homestake. Journal of Physics: Conference Series, 606(1), 26.

Hopp, C., 2023, EGS Collab Experiment 2: Passive seismic monitoring system, Lawrence Berkeley Nat. Lab., LBNL-2001514LBNL EESA, 29 p.

Hyman, J. D., 2020, Flow channeling in fracture networks: Characterizing the effect of density on preferential flow path formation. *Water Resources Research, 56*, e2020WR027986. https:// doi.org/10.1029/2020WR027986

Johnson, T.C., Burghardt, J., Strickland, C., Knox, H., Vermeul, V., White, M., Schwering, P., Blankenship, D. and EGS Collab Team, 2021. 4D Proxy Imaging of Fracture Dilation and Stress Shadowing Using Electrical Resistivity Tomography During High Pressure 132 Injections Into a Dense Rock Formation. Journal of Geophysical Research: Solid Earth, 126(11): e2021JB022298.

Johnson, T., Strickland, C., Burghardt, J., Knox, H., Hopp, C., Rodriguez-Tribaldos, V., Kneafsey, T., Schwering, P., Pope, J., Blankenship, D., Ajo Franklin, J.B. and Pyatina, T., 2022. 3D Electrical Resistivity Characterization and Monitoring at the EGS-Collab Testbed #1: Results and Lessons Learned Applied to Testbed #2, 56th U.S. Rock Mechanics/Geomechanics Symposium, Santa Fe, New Mexico, USA.

Kneafsey, T. J., Blankenship, D., Dobson, P. F., Morris, J. P., White, M. D., Fu, P., Schwering, P. C., Ajo-Franklin, J. B., Huang, L., Schoenball, M., Johnson, T. C., Knox, H. A., Neupane, G., Weers, J., Horne, R., Zhang, Y., Roggenthen, W., Doe, T., Mattson, E., Valladao, C., & EGS Collab Team, 2020, The EGS Collab Project: Learnings from Experiment 1, *45th Workshop on Geothermal Reservoir Engineering, Stanford University, Stanford, California.*

Kneafsey, T., Blankenship, D., Dobson, P., White, M., Morris, J. P., Fu, P., Wu, H., Schwering, P. C., Ajo-Franklin, J. B., Huang, L., Knox, H. A., Neupane, G., Weers, J., Horne, R., Roggenthen, W., Doe, T., & EGS Collab Team, 2021, Fracture Stimulation and Chilled-water Circulation Through Deep Crystalline Rock: Characterization, Modeling, Monitoring, and Heat-transfer Assessment. *46th Workshop on Geothermal Reservoir Engineering, Stanford University, Stanford, California.*

Kneafsey, T.J., Dobson, P.F., Ulrich, C., Hopp, C., Rodríguez-Tribaldos, V., Guglielmi, Y., Blankenship, D., Schwering, P.C., Ingraham M., Burghardt, J.A., White, M.D., Johnson, T.C., Strickland, C., Vermuel, V., Knox, H.A., Morris, J.P., Fu, P., Smith, M., Wu, H., Ajo-Franklin, J.B., Huang, L., Neupane, G., Horne, R., Roggenthen, W., Weers, J., Doe, T.W., Pyatina, T., 2022, The EGS Collab Project – Stimulations at Two Depths, ARMA 22–2261, *56th Rock Mechanics/Geomechanics Symposium Santa Fe, New Mexico, USA.*

Kneafsey, T., Blankenship, D., Burghardt, J., Johnson, T., Dobson, P., Schwering, P., Hopp, C. White, M., Morris, J. Strickland, C., Vermuel, V., Fu, P., Ingraham, M., Roggenthen, W., Doe, T., Ajo-Franklin, J., Huang, L., Rodríguez-Tribaldos, V., Guglielmi, Y., Knox, H., Cook, P., Soom, F., Ulrich, C., Frash, L., Neupane, G., Pyatina, T., Weers, J., Mattson, E., Robertson, M., and The EGS Collab Team, 2023,, The EGS Collab – Discoveries and Lessons from an Underground Experiment Series, *PROCEEDINGS 48th Workshop on Geothermal Reservoir Engineering Stanford University, Stanford, California, February 6-8, 2023 SGP-TR-224*

Kneafsey, T., Johnson, T., Burghardt, J., Schwering, P., Frash, L., Roggenthen, W., Hopp, C., Neupane, G., Mattson, E., Ulrich, C., Soom, F., Doe, T., Weers, J., Artz, T., Robertson, M. and EGS Collab Team, 2024, The EGS Collab Project – Summaries of Experiments 2 and 3: Experiments at 1.25 km depth at the Sanford Underground Research Facility. Lawrence Berkeley National Laboratory, *LBL Publications*, Permalink https://escholarship.org/uc/item/43k0p074 , 307 p.

Kumar, S., Singh, B., Banerjee, P., and S. Raval, A review of laser scanning for geological and geotechnical applications in underground mining, 2023, International Journal of Mining Science and Technology, 33, p. 133–154.

Mitchell, S. T., 2010, *Nuggets to Neutrinos: The Homestake Story*, Xlibris Corporation, ISBN 1456839470, 9781456839475, 711 p.

Noble, James A., 1948, High-Potash dikes in the Homestake Mine, Lead, South Dakota, *Bull. Geol. Soc. Amer.,* v. 59, p . 927-940.

Schwering, P., Ingraham, M., Vermeul, V., Burghardt, J., Johnson, T., Strickland, C., White, M., Hopp, C., Tribaldos, V.R., Kneafsey, T., Artz, T., Mattson, E., Doe, T., and Team*, E.C., 2023. Shut-In Testing on the 4100L - Implications on the State of Stress, Fractures, and Wellbores in the Second EGS Collab Testbed, 48th Workshop on Geothermal Reservoir Engineering, Stanford University, Stanford, California.

Singh, S. K. , Banerjee, B. P. , Raval, S., 2023, A review of laser scanning for geological and geotechnical applications in underground mining, *International Journal of Mining Science and Technology*, 33, p. 133–154.

Stetler, L. D., 2015. Water geochemistry and pressure buildup in drill holes on the 4850-ft level at the Sanford underground research laboratory. *Proceedings of the South Dakota Academy of Science*, v. 94, p 317-327.

Ulrich, C., Dobson, P.F., Kneafsey, T.J, Roggenthen, W.M., Uzunlar, N., Doe, T.W., Neupane, G., Artz, T., Dobler, K., Schwering, P., Smith, M., and Burghardt, J.A., 2022, Characterizing rock fractures and physical properties for Experiment 2 of the EGS Collab Project, Sanford Underground Research Facility, ARMA 22-341, *56th Rock Mechanics/Geomechanics Symposium Santa Fe, New Mexico, USA*.

White, M. D., P. Fu, A. Ghassemi, H. Huang, J. Rutqvist, B. Johnston, and the EGS Collab Team, 2018, Numerical Simulation Applications in the Design of EGS Collab Experiment 1, in *PROCEEDINGS, 43rd Workshop on Geothermal Reservoir Engineering*, edited, Stanford University, Stanford, California